Journal of Materials Chemistry A

Accepted Manuscript

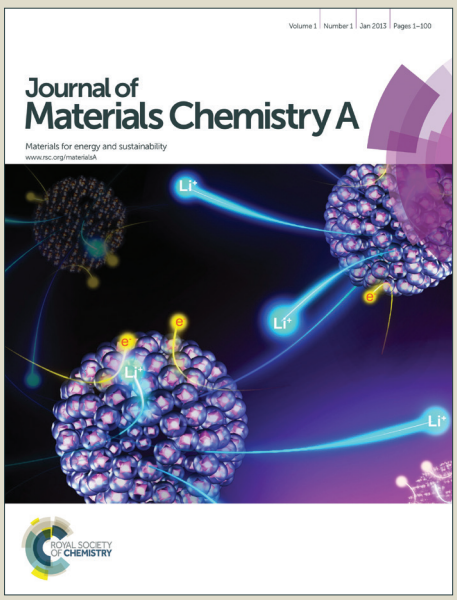

This is an *Accepted Manuscript*, which has been through the Royal Society of Chemistry peer review process and has been accepted for publication.

Accepted Manuscripts are published online shortly after acceptance, before technical editing, formatting and proof reading. Using this free service, authors can make their results available to the community, in citable form, before we publish the edited article. We will replace this *Accepted Manuscript* with the edited and formatted *Advance Article* as soon as it is available.

You can find more information about *Accepted Manuscripts* in the Information for Authors.

Please note that technical editing may introduce minor changes to the text and/or graphics, which may alter content. The journal's standard Terms & Conditions and the Ethical guidelines still apply. In no event shall the Royal Society of Chemistry be held responsible for any errors or omissions in this *Accepted Manuscript* or any consequences arising from the use of any information it contains.

ROYAL SOCIETY OF CHEMISTRY

www.rsc.org/materialsA

Graphical abstract: Co(OH)2 arrays/GNSs composites are constructed by preferentially oriented growth and exhibit a high-performance used as anode materials for lithium-ion batteries.

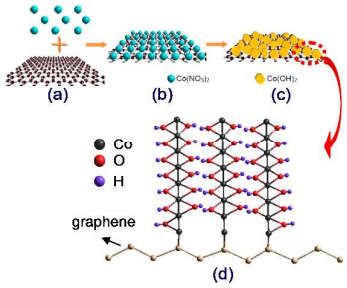

Journal of Materials Chemistry A Accepted Manuscript

Journal of
Materials Chemistry A

Cite this: DOI: 10.1039/c0xx00000x

ARTICLE TYPE

www.rsc.org/xxxxxx

Free-Standing Cobalt Hydroxide Nanoplatelet Array Formed by Growth of Preferential-Orientation on Graphene Nanosheets as Anode Material for Lithium-Ion Batteries

Jisheng Zhou, [a,b] Jingming Li, [a] Kunhong Liu,[c] Ling Lan, [c] Huaihe Song,*[,a] and Xiaohong Chen[a]

Received (in XXX, XXX) Xth XXXXXXXXX 20XX, Accepted Xth XXXXXXXXX 20XX
DOI: 10.1039/b000000x

Cobalt hydroxide arrays/graphene nanosheets ($Co(OH)_2$ array/GNSs) composites are formed by growth of preferential-orientation versus basal planes of GNSs. Notably, the $Co(OH)_2$ nanoplates, possessing special hexagonal morphology with the length of about 130 nm and average thickness of about 20 nm, stand vertically rather than lie flat on the surface of graphene sheets. More interestingly, the (001) crystal plane of $Co(OH)_2$ is vertical to graphene basal plane and forms strong covalent bond interaction (Co-C bond) with graphene layer, which should be driving force for the preferential growth of nanoarrays on graphene. $Co(OH)_2$ array/GNSs composites exhibit not only high specific capacity, but also outstanding high-rate performance when were used as anode material for lithium-ion batteries. At the current density of 50 mAg^{-1}, the reversible capacity is 976 $mAhg^{-1}$ and remains at 1103 $mAhg^{-1}$ after 50 cycles without any fading. At 500 and 1000 mAg^{-1}, the reversible capacities can reach 696 and 496 $mAhg^{-1}$, which are 71 and 51 % of that at 50 mAg^{-1}, respectively. Excellent electrochemical performance should be attributed to the array structure of $Co(OH)_2$ as well as synergistic effect between $Co(OH)_2$ and graphene. Therefore, $Co(OH)_2$ array/GNSs composites are expected to have potential applications in LIBs.

1. Introduction

Cobalt hydroxide, owning unique layered structure as well as excellent electrochemical properties, exhibits great promising application potential in the field of energy storage [1-11]. Traditionally, cobalt hydroxide has long been studied as a key active materials to improve the performance of alkaline storage batteries [1,2]. In recent years, $Co(OH)_2$, as a class of intriguing electrode materials for supercapacitors, exhibits high activity of Faradaic reactions, and high energy and power density [3-8], which has been receiving numerous attention. Very recent reports [9-12] indicate that $Co(OH)_2$ also possesses promisingly high specific capacities when used as anode material in lithium-ion batteries (LIBs). However, the relevant work in the anode area is limited, which may be attributed to an anxiety about "hydrogen" from the hydroxides just as described by the reference [9]. In addition, it can be seen obviously that electrochemical performance of $Co(OH)_2$ from these limited reports needs to be improved urgently for their practical application in further.

Design of novel $Co(OH)_2$ nanostructures or composites in favour of Li-ion diffusions and storage is, therefore, in great need. Due to its outstanding properties, graphene has been regarded as a promising matrix for growing other functional materials as well as for enhancing and/or extending their performance [13]. Many efforts have also been devoted to explore synthesis of novel graphene-based $Co(OH)_2$ architectures for energy storage [9, 11, 14-16]. However, most of $Co(OH)_2$/graphene composites are used as electrode materials for supercapacitors [14-16]. These strategies, aiming toward design of high-performance supercapacitors based on fast surface Faradic reactions, may be not suitable to be employed in advanced anode materials for LIBs storing/releasing energy by repeated solid-state diffusion of Li-ion. In these pioneering work for supercapacitors, it would like to design $Co(OH)_2$ to a two-dimensional structure with the length of several micrometer and the nanoscale thickness offering a high surface area and favourable contacting interface with electrolyte, [13-16] which may be easy to collapse or even peel from current collector during the repeated intercalation/deintercalation of Li-ion. Up to now, there are only two reports on $Co(OH)_2$/graphene composite anode materials for LIBs. [9, 11] The electrochemical performance of the composites has been enhanced largely compared with that of pure $Co(OH)_2$, but there is still a long way to go for their application in future. Therefore, it is still a challenge work for the construction of $Co(OH)_2$/graphene for high-performance anode materials.

It is also an interesting topic to combine both layered materials, graphene and $Co(OH)_2$, into well-designed nanostructures. From the perspective of spatial geometry, growth orientation of layers of $Co(OH)_2$ versus basal plane of GNSs can be divided mainly into two ones. One orientation is that $Co(OH)_2$ layers can be parallel to graphene layers. The other one is that $Co(OH)_2$ layers

Journal of Materials Chemistry A Accepted Manuscript

can be vertical to graphene layers, as shown by Scheme 1. Controlling growth orientations should lead to the construction of various novel nanostructures. Parallel growth of $Co(OH)_2$ layers on graphene will form sheet-on-sheet graphene/$Co(OH)_2$ composites, while, more interesting, vertical growth should construct into $Co(OH)_2$ nanosheet/plate arrays on graphene. In previous reports [17,18], it is suggested that one- or two-dimensional nanoscale *transitional metal oxide* active materials can be assembled into nanoarrays on a substrate to improve their electrochemical performance by enhancing kinetics of Li-diffusion, facilitating the electron conductivity by substrate, and efficiently buffering the volume changes by the nanospace between the arrays. In this regard, it is favourable to enhancing the electrochemical performance of $Co(OH)_2$ by preparation of $Co(OH)_2$ nanosheet/plate arrays on graphene. At present, though there has been a plenty of synthesis studies on $Co(OH)_2$/graphene composites, [9, 11, 14-16] most of $Co(OH)_2$ nanocrystals are only simply dispersed on the graphene and there are very few reports on the preparation of $Co(OH)_2$ arrays on graphene nanosheets. [16] Moreover, there is no report on the design of the nanostructures of $Co(OH)_2$ array based on growth of preferential orientation of hydroxide layers on graphene, especially preferentially vertical orientation of hydroxide layers versus graphene basal plane. There is also no investigation on the key factors affecting the orientation of $Co(OH)_2$ on graphene.

In this work, we construct hexagonal cobalt hydroxide arrays on graphene nanosheets substrate ($Co(OH)_2$ array/GNSs) with vertical orientation of hydroxide layers relative to graphene basal plane by a facile method. The processes involved in the formation of $Co(OH)_2$ array/GNSs are schematically demonstrated in Scheme 1. First, the mixture, where $Co(NO_3)_2$ is dispersed homogeneously on GNSs with less functional groups, is obtained. Then, the $Co(NO_3)_2$ adsorbed on the graphene nanosheets (GNSs) is reacted in situ with KOH solution to form $Co(OH)_2$ arrays with small size of plate. And it was found that the (001) crystal plane of $Co(OH)_2$ is vertical to graphene basal plane and strong interfacial interaction exists between GNSs and $Co(OH)_2$. The key factors affecting on the preferentially orientated growth are also explored. And the nanoarray with interesting structures exhibits superior Li-battery performance when it is used as anode materials for LIBs.

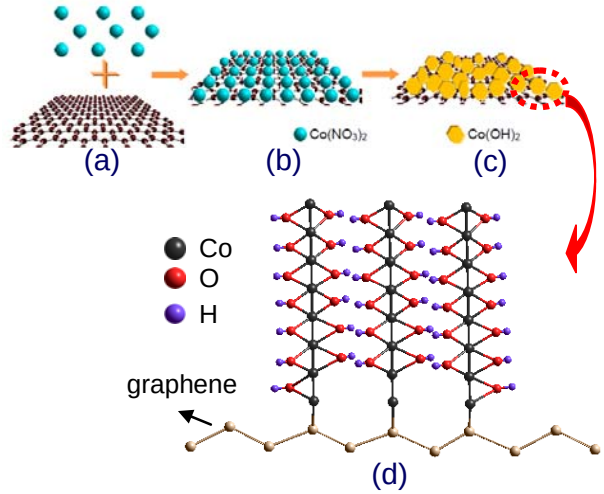

Scheme 1. Schematic illustration of preferentially orientated growth of $Co(OH)_2$ nanoarrays on GNSs.

2. Experimental Section

Preparation of Graphene Nanosheets: The graphene nanosheets (GNSs) were fabricated from natural graphite by the Staudenmaier's method according to our previous work [19]. For comparison, the GNSs were oxidized by HNO_3 (16 mol/L) at 80 ^oC for 6 h. And plenty of functional groups were formed at the surface of GNSs. The original and HNO_3-oxidizing GNSs were used to prepare graphene/ cobalt hydroxide nanosheets in the subsequent experimental procedure.

Fabrication of $Co(OH)_2$/graphene composites and pure $Co(OH)_2$: A facile approach was employed to synthesize hexagonal cobalt hydroxide/graphene composites ($Co(OH)_2$ array/GNSs) at room temperature. Typically, the GNSs (20mg) and $Co(NO_3)_2.6H_2O$ (126.4mg) were well dispersed in ethanol with the help of ultrasonicator KQ-700DE at 700W. Then, after removing ethanol at 80 ^oC under vigorous stirring, the $Co(NO_3)_2$/GNSs composites were obtained. The composites were added to KOH aqueous solution (30 wt%) slowly. After stirring for 10 min, the mixture was transferred into 50 ml funnel, then filtered and washed with deionized water until the PH value was 7. After drying, $Co(OH)_2$ array/GNSs composite was obtained.

For comparison, pure $Co(OH)_2$ without GNSs and $Co(OH)_2$/graphene composites with HNO_3-oxidizing GNSs were also prepared using the same procedure described above.

Characterization: The morphologies and structures of the obtained products were investigated by scanning electron microscope (SEM, ZEISS SUPRA 55), transmission electron microscope (TEM, Hitachi H-800) and high-resolution transmission electron microscope (HRTEM, JEOL JEM-2010).

X-ray diffraction (XRD) measurements were performed with a Rigaku D/max-2500B2+/PCX system using Cu Ka radiation (λ= 1.5406 Å) over the range of 5–90^o (2θ) at room temperature.

The Raman spectra were recorded from 1000 to 2000 cm^{-1} at room temperature using a HR 800 Raman spectrometer (produced by HORIBA Jobin Yvon company) with an excitation line of 532 nm and using an Olympus microscope and a 50×microscopy objective to focus the laser beam onto a spot of 1 μm^2.

Thermogravimetry (TG) and differential scanning calorimetry (DSC) measurements were conducted on a NETZSCH STA449C simultaneous thermal instrument. The samples were heated from room temperature to 1000 ^oC at 5 ^oC /min under flowing air.

X-ray photoelectron energy spectrum (XPS) analysis was carried on using monochromatic AlK (1486.6 eV) X-ray sources with 30 eV pass energy in 0.5 eV step over an area of 650 mm to the sample. All the curve fittings were carried out by using Gaussian-Lorentzian (20%) peak shape after a Shirley background correlation.

The functional groups of the samples were recorded by Fourier transform infrared spectroscopy instrument (FTIR, Thermo Scientific Nicolet iS50).

Electrochemical measurements: The electrochemical experiments of the samples were carried out using 2032-type coin cells. The working electrodes were prepared by mixing active material, acetylene black, and poly (vinyldifluoride) (PVDF) at a weight ratio of 8:1:1 and pasting the mixture onto foam nickel. And counter electrode was lithium sheet. Electrolyte was 1M

Journal of Materials Chemistry A Accepted Manuscript

This journal is © The Royal Society of Chemistry [year]

$LiPF_6$ solution in ethylene carbo-nate/dimethyl carbonate EC-DMC(1:1 v/v). The coin cells were assembled in argon-filled glove box with both moisture and oxygen content below 1 ppm.

Galvanostatic charge–discharge cycling tests were carried out on LAND CT2001A multi-channel battery testing system at various current densities in the voltage range from 0.01 to 3 V at room temperature.

The cyclic voltammetry and electrochemical impedance spectroscopy (EIS) were carried out on a ZAHNER ENNIUM electrochemical working station. For the cyclic voltammetric measurements, the sweep rate was $0.1 mvs^{-1}$ and potential range was from 0.01 V to 3 V. For the EIS measurements, the frequency range was from 0.01 Hz to 100 kHz and the amplitude was 5 mv.

3. Results and Discussion

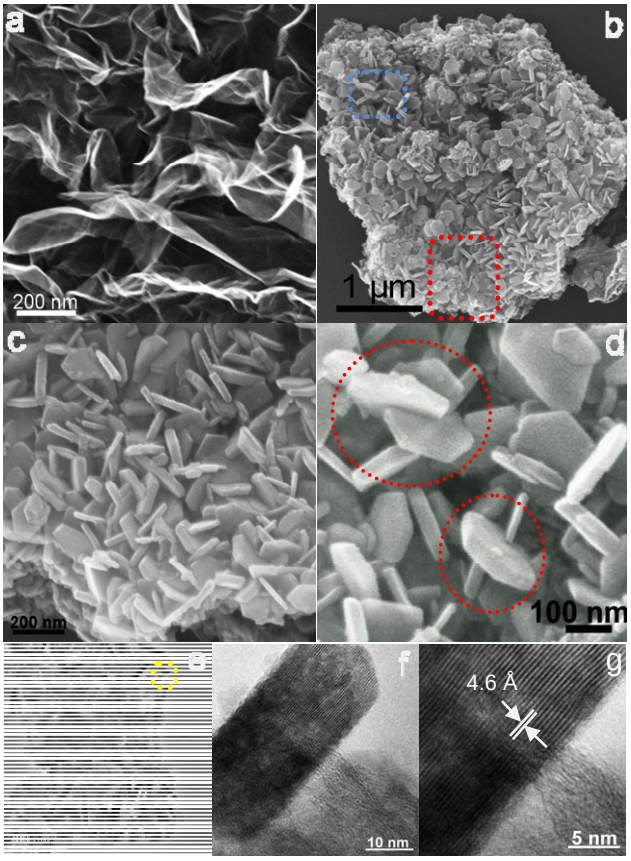

Figure 1. SEM images of (a) GNSs and (b) $Co(OH)_2$ array/GNSs, (c, d) magnifying SEM images in the selected area of red and blue boxes of image (b), (e) HRTEM image of a composite-nanosheet of $Co(OH)_2$ array/GNSs, and (f) HRTEM and (g) clear lattice fringe images of a $Co(OH)_2$ nanosheet standing on the GNSs in the selected area of yellow box of image (e).

Figure 1 exhibits the morphology and structure of original GNSs and as-prepared $Co(OH)_2$array/GNSs composite nanoplates. Two-dimensional GNSs with wave-like structure are almost transparent under the electron beam (Fig. 1a). Fig.1b shows a typical SEM image of $Co(OH)_2$ array/GNSs composite nanoplates. The $Co(OH)_2$ nanoplates possess average width of about 130 nm and average thickness of about 20 nm (Fig. 1c). From the tilted nanoplates as shown in the red circles of Fig. 1d, it can be seen that $Co(OH)_2$ owns very interesting hexagonal structures. Notably, most of these hexagonal nanoplates stand vertically rather than lie flat on the surface of graphene sheets. In addition, the weight content of $Co(OH)_2$ in the composite of $Co(OH)_2$ array/GNSs is approximately 70 wt% calculated from the weight loss in TG measurement (ESI, Fig. S1). Here, it needs to be emphasized that the length of $Co(OH)_2$ nanosheet/wire is around several micrometers or even beyond 10 μm in previous reports [3-12, 14-16]. In contrast, the length of $Co(OH)_2$ nanoplate in this work is much shorter, which will benefit the diffusion of Li-ion and also shorten the length of electronic transfer from active materials to conductive substrate. [20]

HRTEM image of $Co(OH)_2$ array/GNSs composite nanoplates (Fig. 1e) confirms in further the $Co(OH)_2$ nanoplates are vertical to basal plane of GNSs. Therefore, it is very easy to investigate the nanoplate from the side. Interestingly, the side-view HRTEM images (Fig. 1e-g) confirm the well-crystalline lamellar structure of the nanoplate with a interplanar spacing of 4.6 Å, which is in accordance with the (001) crystal plane of $Co(OH)_2$, indicating that the (001) plane composed of a Co layer sandwiched by two OH layers [21] is vertical to graphene basal plane, as shown by Scheme 1d. There is few report on the preparation of $Co(OH)_2$ arrays on graphene nanosheets, [16] but the case, layer-vertical to-layer just like shown here, is never observed directly.

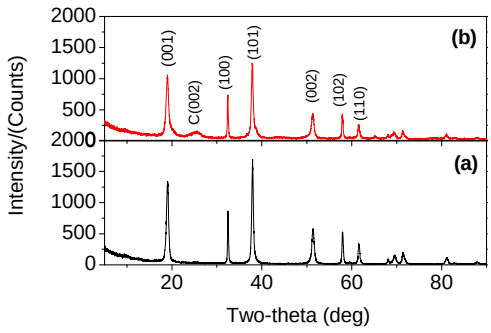

Figure 2. XRD patterns of (a) $Co(OH)_2$ and (b) $Co(OH)_2$ array/GNSs.

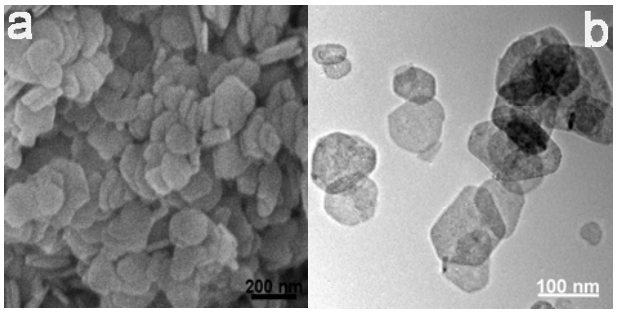

Figure 3. (a) SEM and (b) TEM images of $Co(OH)_2$ nanosheets without GNSs.

For comparison, $Co(OH)_2$ without GNSs is also prepared. Fig. 2a shows the XRD pattern of pure $Co(OH)_2$, in which all of the diffraction peaks are very sharp and indexed well with pure $Co(OH)_2$ and no impurity phases are found, indicating high crystalline degree and high phase purity of $Co(OH)_2$. Compared with $Co(OH)_2$, $Co(OH)_2$ array/GNSs shows a broad C(002) diffraction peak at 25° (Fig. 2b), corresponding to the relative short-range order in stacked graphene sheets. [19] Similarly, both

Journal of Materials Chemistry A Accepted Manuscript

$Co(OH)_2$ nanoplates represent the typical character of a hexagonal phase P-3m1(164), that is brucite-like β-$Co(OH)_2$ phase.[22] Additionally, SEM image (Fig. 3a) shows that pure $Co(OH)_2$ also presents hexagonal plate-like structure, and length and thickness of pure $Co(OH)_2$ are similar with those of nanoplates in $Co(OH)_2$ array/GNSs. The difference is that all of pure $Co(OH)_2$ nanoplate lay flat on the membrane of copper mesh in the vision of TEM measurement, and no standing nanoplate is observed, which is similar to that in previous reports. [9-12,14] It can be deduced that GNSs play an important role in the preferentially oriented growth of $Co(OH)_2$ in the hybrids.

It is interesting to consider what controls the preferentially oriented growth of $Co(OH)_2$ nanoplates on the GNSs. In previous reports, graphene oxide (GO) with plenty of oxygen-containing functional groups was usually used as matrix to prepare the graphene-based cobalt hydroxide composites. [9, 11, 14, 15] In these composites used GO as matrix, $Co(OH)_2$ nanosheets/plates generally lay flat on GNSs. Dai et al. [23] suggested that oxidation degree of graphene could affect the morphology of metal hydroxide nanocrystals. Compared this work with previous reports, [9, 11, 14, 15] it can be deduced that orientation of $Co(OH)_2$ versus GNSs should also be related to the functional groups. To confirm the influence of surface nature on growth of $Co(OH)_2$ nanoplate in further, GNSs after oxidization by HNO_3 (GNSs-HNO_3), owning plenty of –COOH functional groups (ESI, Fig. S2), was also used to prepare graphene-based $Co(OH)_2$ composites ($Co(OH)_2$/GNSs-HNO_3). Surprisingly, it can be found that all of hexagonal $Co(OH)_2$ lay flat on rather than stand on the GNSs (ESI, Fig. S2 and S3). Our results imply obviously that surface nature of GNSs will control the preferentially orientation growth of $Co(OH)_2$ nanoplates on the GNSs due to that surface nature affect the interfacial reaction and interaction between metal hydroxide and graphene.

To clarify the interfacial nature between GNS and standing $Co(OH)_2$ nanosheets, Raman measurements were carried out (Figure 4). It indicates the existence of obvious interfacial interaction between GNSs and $Co(OH)_2$. The intensity ratio of D band to G band (I_D/I_G) is usually used to confirm the order degree of graphene layers. The value of I_D/I_G (ESI, Table S1) for GNSs is ca. 0.96, while that of composite increases to ca. 1.04, indicating that the $Co(OH)_2$ on GNSs leads to the increased disorder of graphene layers, which should be attributed to the destruction of continuity of π network of graphene by the interfacial interaction between $Co(OH)_2$ and GNSs. [24]

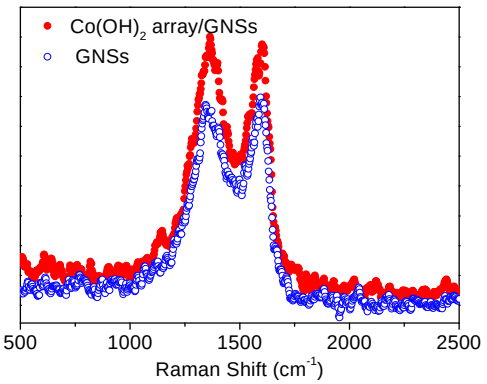

Figure 4 Raman spectra of GNSs and $Co(OH)_2$ array/GNSs.

More valuable information for interfacial nature can be obtained by X-ray photoelectron spectroscopy (XPS) measurement just as shown by our previous work. [24] Overall XPS spectra in Fig 5.(a) show that GNSs are composed of both C and O elements, while $Co(OH)_2$ array/GNSs composites are composed of C, O and Co elements. The C1s spectra of GNSs can be decomposed into the dominant peak at 284.6 eV to C=C/C-C, and other three peaks of oxygen-containing functional groups at 286.1 eV to C-O, 287.3 eV to C=O, and 289.5 eV to O-C=O, respectively. [25] Besides four peaks of C=C/C-C and oxygen-containing peaks, a new peak in C1s spectrum of $Co(OH)_2$ array/GNSs is presented at 283.1 eV, which should be attributed to Co-C bond according to previous reports.[26] Correspondingly, a peak at 778.6 eV, ascribed to Co-C bond, [26] can also be observed in the spectrum of $Co2p_{3/2}$ in Fig. 5 (c).

In Figure 5(d), the O1s spectra were fitted to two peaks. The peak at 533.3eV refers to C-O bond, and the other peak in the spectrum of GNSs at 531.2eV should be attributed to C=O/O-C=O. [25] Compared with that in GNSs, the intensity of peak at 531.2 eV in the composites increases largely. Generally, the peak of O1s in $Co(OH)_2$ is present at ca. 531.2 eV.[27] In addition, O1s peak in the C-O-Metal bond is located at ca. 531-533 eV in previous reports. [24, 28] However, content of C contacting with oxygen is not increased, so the peak at 531.2 eV in the composites should be attributed to only both C=O and $Co(OH)_2$. (ESI, Table S2) The possibility for formation of C-O-Co bond is ruled out.

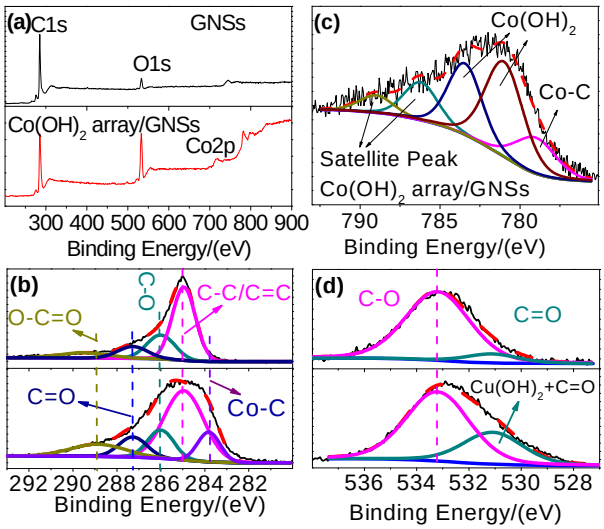

Figure 5. (a) XPS spectra of GNSs and $Co(OH)_2$ array/GNSs, and their (b) C1s, (c) $Co2p_{3/2}$, and (d) O1s spectra.

The $Co(OH)_2$/GNSs-HNO_3 composites exhibit absolutely different interfacial nature by comparing their XPS spectra with those of the $Co(OH)_2$ array/GNSs (ESI, Fig. S4). In the C1s spectrum of $Co(OH)_2$/GNSs-HNO_3 (ESI, Fig. S4b), no peak of Co-C bonds at 283.1 eV is presented except four peaks of C=C/C-C and oxygen-containing peaks. Likewise, the peak at 778.6 eV, corresponding to Co-C bonding, is also not appeared in the $Co2p_{3/2}$ spectrum of $Co(OH)_2$/GNSs-HNO_3 (ESI, Fig. S4c). Compared with O1s spectrum of $Co(OH)_2$ array/GNSs (ESI, Fig. S4d), it can be found, besides C-O peak at 533.3 eV and the peak at 531.2 eV from C=O and $Co(OH)_2$, that a new peak at 531.9 eV is presented in the O1s spectrum of $Co(OH)_2$/GNSs-HNO_3, which

Journal of Materials Chemistry A Accepted Manuscript

This journal is © The Royal Society of Chemistry [year]

should be attributed to C-O-Co binding according to previous reports. [24, 28]

Based on the XPS results above, interfacial interaction of Co-C covalent bond exists in the $Co(OH)_2$ array/GNSs, while C-O-C binding connection is the $Co(OH)_2$/GNSs-HNO_3. The C-O-Co binding formation should be attributed to the reaction between basic hydroxyl planes of the brucite plates and plenty of –COOH acidic groups in GO, according to very recent reports. [15, 29] Considering that the layer-structure of $Co(OH)_2$ is a Co layer sandwiched by two OH layers, $Co(OH)_2$ nanosheets/plates are, therefore, more apt to grow flatly along the basic plane of GNSs in the previous work based on GO as matrix [14-16] as well as GNSs oxidized by HNO_3 in this work (ESI, Fig. S2 and S3). In contrast, Co-C binding formation in $Co(OH)_2$ array/GNSs indicates that GNSs can connect preferentially with end face of $Co(OH)_2$ nanosheets. Banhart et al. have revealed that metal atoms can be bonded with graphene, especially with the defect.[30] Simultaneously, if considering the sandwiched Co layer structure of $Co(OH)_2$, it is easy to understand that Co-C bond can be formed by bonding between bare Co atoms at the end face of $Co(OH)_2$ and defects of GNSs. Model of interaction can be schematically demonstrated in **Scheme 1e**. $Co(OH)_2$ nanosheets/plates are, therefore, more apt to grow vertically on the basic plane of GNSs. Here, the interfacial interaction of Co-C bond between GNSs and $Co(OH)_2$ as well as nanoarray-like construction will be helpful to the improvement of electrochemical performance of $Co(OH)_2$ as anode materials for LIBs.

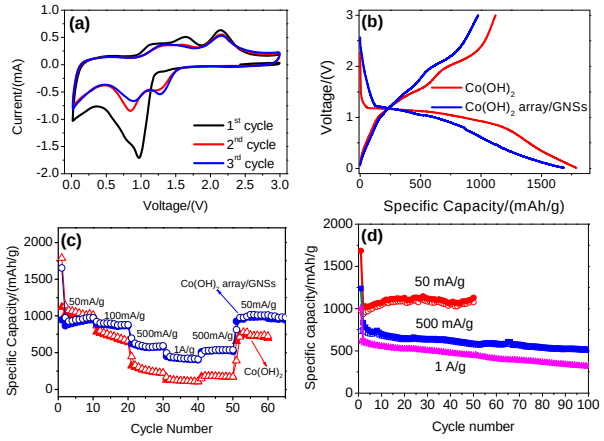

Figure 6. (a) Cyclic voltammograms of the $Co(OH)_2$array/GNSs at scan rate of 0.1 mV s^{-1}, (b) the initial discharge-charge curve of $Co(OH)_2$ and $Co(OH)_2$array/GNSs at 50 mAg^{-1}, (c) the rate-performance of $Co(OH)_2$ and $Co(OH)_2$array/GNSs at various current densities, and (b) the cyclic performance of $Co(OH)_2$array/GNSs at various current densities.

The electrochemical activity of $Co(OH)_2$ array/GNSs as anode materials is measured by cyclic voltammograms (CV) at room temperature (Fig. 6a). In the first cycle, a large cathodic current peak appears centred at ca. 1.0 V and followed by two weak anodic peaks centred at ca. 1.14 and 1.64 V, respectively, and a strong one at ca. 2.06 V. The cathodic peak at ca. 1.0 V should be attributed to the reduction to Co^{2+} of $Co(OH)_2$ to Co^0 as well as the formation of solid electrolyte (SEI) films, while the three anodic peaks are ascribed to the multistep reactions of oxidation of Co^0 to Co^{2+} according to previous reports. [9-12] Compared with the 1st cycle, a new cathodic peak appears at 1.28V and a new anodic peak appears at 1.33 V. At the same time, anodic peak at 1.14 and 1.64 V disappears in the second cycle. And the both anodic and cathodic peaks of third cycle are consistent with those of second cycle, indicating that stable reversible electrochemical reaction has been set up. We note that the CV curves for the second and third cycles in this work are obviously different from those of $Co(OH)_2$ with large area in the previous work, [11] where both anodic and cathodic peaks of the second and third cycles are nearly consistent with those of the first cycle, indicating the different mechanism of lithium storage. This may be attributed to the size of active materials just as shown in the work of Tarascon et al.,[31] which suggested that Li-ion storage mechanism of bulk iron oxide is different from that of nanoscale iron oxide. However, the exact reason for the difference is unclear due to limited report for Li-storage in $Co(OH)_2$, [9-12] so investigation in detail is needed in the following work.

In further, we evaluated the cyclic stability and rate-performance of $Co(OH)_2$ and $Co(OH)_2$array/GNSs by charge-discharge measurements. Fig. 6b shows the first discharge/charge voltage profiles of $Co(OH)_2$array/GNSs and pure $Co(OH)_2$ at current density of 50 mAg^{-1}. Their discharge/charge curves are very alike, where one long discharge plateau from 1.2 to 0.8 V, and three obvious charge plateaus (1.0-1.5 V, 1.5-2.0 V and 2.0-2.5 V) are clearly observed, which are consistent with the CV measurements. For pure $Co(OH)_2$, the initial discharge (Li-insertion) and charge (Li-desertion) capacities are 1787 and 1120 $mAhg^{-1}$, respectively. Rate-performance of pure $Co(OH)_2$ nanoplates is also exhibited in Fig. 6c. The delivered capacities of $Co(OH)_2$ nanoplates at 100, 500, and 1000 mAg^{-1} are ca. 788, 321, and 124 $mAhg^{-1}$, respectively. After the current density returns to 50 mAg^{-1}, the specific capacity can recover to ca. 743 $mAhg^{-1}$ and keep at 697 $mAhg^{-1}$ after 60 cycles, which is ca. 62 % of the first reversible capacity. Compared with previous reports, [9-12] it can be concluded that specific capacity and rate-performance of $Co(OH)_2$ plates with nanoscale length are also better than that of large area $Co(OH)_2$ sheets. For example, the work by He et al. [9] showed that the reversible capacity of $Co(OH)_2$ sheets with discal size of ca. 0.65 μm diameter was ca. 660 $mAhg^{-1}$ and no corresponding rate-performance was measured. At Huang's paper [10], reversible capacity of pure $Co(OH)_2$ sheets with size of ca. 1-3 μm was 912 $mAhg^{-1}$ at first cycle and 63 $mAhg^{-1}$ after 50 cycles at 58 mAg^{-1}, and decreased to ca. 30 $mAhg^{-1}$ at 1160 mAg^{-1}. These results indicate that the plates with nanoscale diameter possess higher electrochemical activity and are more in favour of diffusion of Li-ion.

Compared with the electrochemical performance of pure $Co(OH)_2$ sheets, $Co(OH)_2$ array/GNSs composites exhibit not only high cyclic stability, but also better high-rate performance. At 50 mAg^{-1}, the first discharge and charge capacities are 1654 and 977 $mAhg^{-1}$, respectively. At higher current densities of 100, 500, and 1000 mAg^{-1}, the reversible capacities can reach up to 925, 696 and 496 $mAhg^{-1}$, which maintain about 95, 71 and 51 % of capacities at 50 mAg^{-1}, respectively. After the current density returns to 50 mAg^{-1}, the reversible capacity can be still up to ca. 980 $mAhg^{-1}$, and there is no any capacity fade after 65 cycles. It can also be calculated that the capacity contributed by $Co(OH)_2$ is ca.1237 $mAhg^{-1}$ by capacities of composite (980 $mAhg^{-1}$) and GNSs (381 $mAhg^{-1}$ after 50 cycles, see the ESI, Fig. S5), and

Journal of Materials Chemistry A Accepted Manuscript

weight content of $Co(OH)_2$, indicating that GNSs can be beneficial for large improvement of electrochemical activity of $Co(OH)_2$.

Moreover, Fig. 6d reveals the cyclic performance of $Co(OH)_2$ array/GNSs at various current densities using three new cells. At 50 mAg^{-1}, there is still no capacity fade, indicating better repeatability of $Co(OH)_2$ array/GNSs. When the cell is discharged/charged directly at a higher current density of 500 mAg^{-1}, the first reversible capacity still reach to 734 $mAhg^{-1}$, and reversible capacity keeps at ca. 508 $mAhg^{-1}$ after 100 cycles, which is ca. 69 % of the first reversible capacity. At 1 Ag^{-1}, the first reversible capacity still reach to 615 $mAhg^{-1}$, and reversible capacity keeps at ca. 321 $mAhg^{-1}$ after 50 cycles, which is ca. 52 % of the first reversible capacity. It can be seen that both the specific capacity and cyclic stability of $Co(OH)_2$array/GNSs at high rate are also superior to the reported values of $Co(OH)_2$ nanosheets as well as graphene-based $Co(OH)_2$ hybrids. [9-12] And the electrochemical performance $Co(OH)_2$array/GNSs is even comparable with those of graphene-based cobalt oxide anode materials. [32]

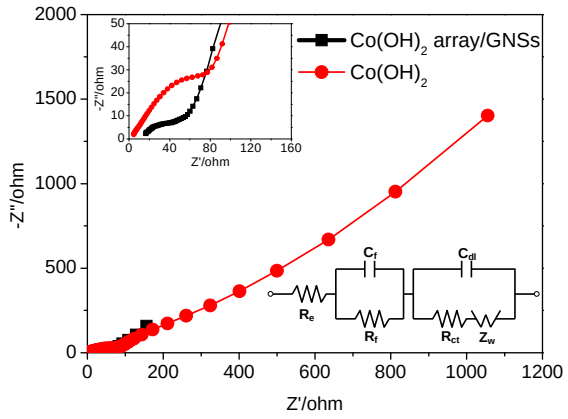

Figure 7. EIS spectra of $Co(OH)_2$ and $Co(OH)_2$array/GNSs after 50 cycles at current density of 50 mAg^{-1} and equivalent circuit for EIS simulation (inset in the Figure).

Measurements of Electrochemical impedance spectroscopy (EIS) reveal the kinetic information of Li-ion storage in pure $Co(OH)_2$ sheets and $Co(OH)_2$ array/GNSs composites (Fig. 7). EIS is constituted of two semicircles in the high frequency region and an inclined line at low frequency. Generally, the radius of the semicircle represents contact and charge-transfer impedances and the slope of the line reflects Warburg resistance, which reveals the diffusion of redox species in the electrolyte. The elements in the equivalent circuit include the ionic resistance of electrolyte (R_e), the intrinsic resistance of SEI-solid electrolyte interface (R_f) and charge-transfer resistance (R_{ct}) between the electrode and electrolyte. According to the simulation by equivalent circuit (inset in Fig. 7), the value of R_f of $Co(OH)_2$array/GNSs and $Co(OH)_2$ is 7.8 and 9.2Ω, while their R_{ct} values are 11.7 and 35.8 Ω, respectively. R_{ct} value of $Co(OH)_2$ array/GNSs is much lower than that of $Co(OH)_2$, indicating that GNSs addition and the interfacial interaction between GNSs and $Co(OH)_2$ improve largely the conductivity of $Co(OH)_2$. In addition, the hexagonal structure of $Co(OH)_2$ as well as the special conjunction between $Co(OH)_2$ and GNSs should also help to improve the electrochemical stability of composite.

Conclusions

In present work, we prepared graphene-based $Co(OH)_2$ composite nanosheets by a facile in-situ reaction between $Co(NO_3)_2$ on GNSs and KOH. The composites own very interesting structure that the hexagonal $Co(OH)_2$ nanoplates stand on graphene basal plane rather than lay flat on graphene, and (001) crystal planes of $Co(OH)_2$ nanoplates are preferentially vertical orientation versus graphene basal plane and interact with graphene by Co-C covalent bonds. The $Co(OH)_2$array/GNSs composite exhibits high specific capacitance and better rate-performance. We attribute promising electrochemical performance to the particular structure of $Co(OH)_2$ as well as synergistic effect between $Co(OH)_2$ and graphene. Therefore, $Co(OH)_2$array/GNSs are expected to have potential applications in LIB.

This work was supported by the National Natural Science Foundation of China (51202009 and 51272019), New Teachers' Fund for Doctor Stations, Ministry of Education of China (20120010120004), Natural Science Foundation of Jisangsu Province of China (SBK2014040036), and Foundation of Excellent Doctoral Dissertation of Beijing City (YB20121001001).

Notes and references

[a] *State Key Laboratory of Chemical Resource Engineering, Beijing Key Laboratory of Electrochemical Process and Technology for Materials, Beijing University of Chemical Technology, Beijing, P. R. China. Fax:+86 10-64434916; Tel: +86 10-64434916; E-mail: songhh@mail.buct.edu.cn*

[b] *Changzhou Institute of Advanced Materials, Beijing University of Chemical Technology, Jiangsu, P. R. China.*

[c] *Petrochemical Research Institute, PetroChina Company Limited, Beijing, 100195, P. R. China*

† Electronic Supplementary Information (ESI) available: Detailed experimental procedures; TG and DSC curves of the $Co(OH)_2$array/GNSs composites, FTIR spectra of original GNSs and GNSs oxidized by HNO_3, SEM image schematic illustration of hexagonal $Co(OH)_2$ nanoplates on HNO_3-oxidizing GNSs, data for Raman spectra and C1s XPS spectra, and cyclic performance of GNSs as anode materials. See DOI: 10.1039/b000000x/

1 S. U. Falk, and A. J. Salkind, Alkaline Storage Batteries, Wiley, New York, 1969, 54.
2 W. Y. Li, S. Y. Zhang and J. Chen, *J. Phys. Chem. B*, 2005, **109**, 14025.
3 L. Cao, F. Xu, Y.-Y. Liang and H.-L. Li, *Adv. Mater.*, 2004, **16**, 1853.
4 C. Yuan, L. Hou, L. Shen, D. Li, F. Zhang, C. Fan, J. Li, X. Zhang, *Electrochim. Acta*, 2010, **56**, 115.
5 J.-K. Chang, C.-M. Wu and I-W. Sun, *J. Mater. Chem.*, 2010, **20**, 3729.
6 R. S. Jayashree and P. V. Kamath, *J. Mater. Chem.*, 1999, **9**, 961.
7 H. Hosono, S. Fujihara, I. Honma, M. Ichihara and H. Zhou, *J. Power Sources*, 2006, **158**, 779.
8 W.-J. Zhou, J. Zhang, T.Xue, D.-D. Zhao and H.-L. Li, *J. Mater. Chem.*, 2010, **2008**, 18, 905.
9 Y.-S. He, D.-W. Bai, X. Yang, J. Chen, X.-Z. Liao and Z.-F. Ma, *Electrochem. Comm.* , 2010, **12**, 570.
10 X. L. Huang, X. Zhao, Z.-L. Wang, L. M. Wang and X. B. Zhang, *J. Mater. Chem.*, 2012, **22**, 3764.
11 X. L. Huang, J. Chai, T. Jiang, Y.-J. Wei, G. Chen, W.-Q. Liu, D. Han, L. Niu, L. Wang and X.-B. Zhang, *J. Mater. Chem.*, 2012, **22**, 3404.

This journal is © The Royal Society of Chemistry [year]

Journal of Materials Chemistry A Accepted Manuscript

12 E. Chen, Fu, M. Zhou, Y. Xu, L. Fei, S. Deng, V. Chaitanya, Y. Wang and H. Luo, *J. Alloys Compounds*, 2013, **578**, 349.

13 K. S. Novoselov, A. K. Geim, S. V. Morozov, D. Jiang, Y. Zhang, S. V. Dubonos, I. V. Grigorieva and A. A. Firsov, *Science*, 2004, **306**, 666; M. J. Allen, V. C. Tung and R. B. Kaner, *Chem. Rev.*, 2010, **110**, 132.

14 S. Chen, J. Zhu and X. Wang, *J. Phys. Chem. C*, 2010, **114**, 11829; C. M. Zhao, X. Wang, S. Wang, Y. Y. Wang, Y. X. Zhao and W. T. Zheng, *International journal of hydrogen energy*, 2012, **37**, 1146; C. Zhao, W. Zhang, X. Wang, H. Zhang, X. Cui and H. Wang, *Sci. Rep.*, 2013, **3**, 2986; Z. Li, J. Wang, L. Niu, J. Sun, P. Gong, W. Hong, L. Ma and S. Yang, *J. Power Sources*, 2014, **245**, 224.

15 C. Nethravathi, C. R. Rajamathi, M. Rajamathi, X. Wang, U. K. Gautam, D. Golberg and Y. Bando, *ACS Nano*, 2014, **8**, 2775; D. Ghosh, S. Giri and C. K. Das, *ACS Sustainable Chem. Eng.*, 2013, **1**, 1135; C.-Y. Sun, Y.-G. Zhu, T.-J. Zhu, J. Xie, G.-S. Cao and X.-B. Zhao, *J Solid State Electrochem.*, 2013, **17**, 1159.

16 Q. Cheng, J. Tang, N. Shinya and L.-C. Qin, Sci. *Technol. Adv. Mater.*, 2014, **15**, 014206.

17 P. L. Taberna, S. Mitra, P. Poizot, P. Simon and J.-M. Tarascon, *Nat. Mater.*, 2006, **5**, 567; J. Jiang, Y. Y. Li, J. P. Liu, X. T. Huang, C. Z. Yuan and X. W. Lou, *Adv. Mater.*, 2012, **24**, 5166; S. C. Zhang, Z. J. Du, R. X. Lin, T. Jiang, G. R. Liu, X. M. Wu and D. S. Weng, *Adv. Mater.*, 2010, **22**, 5378–5382; F. F. Cao, J. W. Deng, S. Xin, H. X. Ji, O. G. Schmidt, L. J. Wan and Y. G. Guo, *Adv. Mater.*, 2011, **23**, 4415.

18 J. Zhu, Y. K. Sharma, Z. Zeng, X. Zhang, M. Srinivasan, S. Mhaisalkar, H. Zhang, H. H. Hng and Q. Yan, *J. Phys. Chem. C*, 2011, **115**, 8400.

19 P. Guo, H. Song and X.Chen, *Electrochem. Commun.*, 2009, **11**, 1320.

20 P. G. Bruce, B. Scrosati and J.-M.Tarascon, *Angew. Chem. Int. Ed.*, 2008, **47**, 2930.

21 Y. Hou, H. Kondoh, M. Shimojo, T. Kogure and T. Ohta, *J. Phys. Chem. B*, 2005, **109**, 19094.

22 J. T. Sampanthar and H. C. Zeng, *J. Am. Chem. Soc.*, 2002, **124**, 6668; X. W. Lou, D. Deng, J. Y. Lee, J. Feng, L and A. Archer, *Adv. Mater.*, 2008, **20**, 258; Z. Liu, R. Ma, M. Osada, K. Takada and T. Sasaki, *J. Am. Chem. Soc.*, 2005, **127**, 12869.

23 H. Wang, J. T. Robinson, G. Diankov and H. Dai, J. Am. Chem. Soc., 2010, 132, 3270-3271.

24 J. Zhou, H. Song, L. Ma and X. Chen, *RSC Adv.*, 2011, **1**, 782 ; X. Zhang, J. Zhou, H. Song, X. Chen, Y. V. Fedoseeva, A. V. Okotrub, and L. G. Bulusheva, *ACS Appl. Mater. Interfaces*, 2014, **6**, 17236 ; G. M. Zhou, D. W. Wang, L. C. Yin, N. Li, F. Li, H.M. Cheng, *ACS Nano,* 2012, **6**, 3214.

25 C. Mattevi, G. Eda, S. Agnoli and S. Miller, *Adv. Funct. Mater.*, 2009, **19**, 2577; A. Bagri, C. Mattevi, M. Acik, Y. J. Chabal, M. Chhovalla and V. B. Shenoy, *Nat. Chem.*, 2010, **2**, 581.

26 H. Wang, M. F. Chiah, W. Y. Cheung and S. P. Wong, *Phys. Lett. A*, 2003, **316**, 122; D.-X. Ye, S. Pimanpang, C. Jezewski, F. Tang, J. J. Senkevich, G.-C. Wang and T.-M. Lu, *Thin Solid Films*, 2005, **485**, 95; X.-H. Wang, M.-H. Zhang, W. Li and K.-Y. Tao, *Dalton Trans.*, 2007, 5165-5170; H. Wang, S. P. Wong, W. Y. Cheung, N. Ke, W. F. Lau, M. F. Chiah and X. X. Zhang, *Mater. Sci. Eng. C*, 2001, **16**, 147.

27 J. Yong, H. Liu, W. N. Martens and R. L. Frost, *J. Phys. Chem. C*, 2010, **114**, 111; N. S. Mclntyre and M. G. Cook, *Analy Chem.*, 1975, **47**, 2208; J.-C. Dupin, D. Gonbeau, P. Vinatier and A. Levasseur, *Phys. Chem. Chem. Phys.*, 2000, **2**, 1319; C. Zhao, X. Wang, S. Wang, Y. Wang, Y. Zhao and W. Zheng, *Int. J. Hydrogen Energy*, 2012, **37**, 11846.

28 G. Kataby, M. Cojocaru, R. Prozorov and A. Gedanken, *Langmuir*, 1999, **15**, 1703; C. Combellas, M. Delamar, F. Kanoufi, J. Pinson and F. I. Podvorica, *Chem. Mater.*, 2005, **17**, 3968. B. L. Hurley and R. L. McCreery, *J. Electrochem. Soc.*, 2004, **151**, B252; S. Serghini-Monim, P. R. Norton, R. J. Puddephatt, K. D. Pollard and J. R. Rasmussen, *J. Phys. Chem. B*, 1998, **102**, 1450; C. Dicke, M. Morstein and G. Hahner, *Langmuir*, 2002, **18**, 336.

29 Z. Wu, X.-L. Huang, Z.-L. Wang, J.-J. Xu, H.-G. Wang and X.-B. Zhang, *Sci. Rep.*, 2014, doi:10.1038/screp03669.

30 J. A. Rodríguez-Manzo, O. Cretu and F. Banhart, *ACS Nano*, 2010, **4**, 3422.

31 D. Larcher, C. Masquelier, D. Bonnin, Y. Chabre, C. Masson, J.-B. Leriche and J.-M. Tarascon. *J. Electrochem. Soc.*, 2003, **150**, A133.

32 Z.-S. Wu, W. Ren, L. Wen, L. Gao, J. Zhao, Z. Chen, G. Zhou, F. Li and H.-M. Cheng, *ACS Nano*, 2010, **4**, 3187; H. Kim, D. H. Seo, S. W. Kim, J. Kim and K. Kang, *Carbon*, 2011, **49**, 326; B. J. Li, H. Q. Cao, J. Shao, G. Q. Li, M. Z. Qu and G. Yin, *Inorg. Chem.*, 2011, **50**, 1628; J. Zhu, Y. K. Sharma, Z. Zeng, X. Zhang, M. Srinivasan, S. Mhaisalkar, H. Zhang, H. H. Hang and Q. Yang, *J. Phys. Chem. C*, 2011, **115**, 8400.

Journal of Materials Chemistry A Accepted Manuscript